

A New Approach to Electric Vehicle Charging using a Wireless Method

Mokara Aditya¹, M Sai Prudhvi Raj², Munaga Prudhvi Kumar³,

Kaviti Pavankumar⁴, Gidijala Ramesh Kumar⁵

Students, Department of Mechanical Engineering^{1,2,3,4,5}

GMR Institute of Technology, Rajam, Andhra Pradesh, India

Abstract: Electric cars must be recharged at power stations using a plug-in or static wireless charging technique. It takes longer to recharge, and some locations have no local power stations. Even if electric vehicles are currently a dominant force in the transportation sector, there are certain disadvantages. The main drawback of electric vehicles is the charging system, and because plug-in charging is an old technique, many companies have switched to wireless charging. However, there is one similarity between wireless and plug-in charging: both recharge vehicles while they are in a static position. Dynamic wireless charging is a new technique that can speed up vehicle charging and saves the battery charging wait time. Vehicles can be charged while it moving on the road resulting in the reduction of battery size. Dynamic wireless charging (DWC) technology is an innovation that is attracting the electric vehicle (EV) sectors because of its ability to solve several problems, including messy cables, safety concerns in wet situations, battery size issues, and battery charging wait times.

Keywords: Wireless Power Transfer, Compensation topologies, coil design

I. INTRODUCTION

To find a more dependable and useful option, the wireless charging strategy has been researched. Electric car wired charging systems are very efficient, but their primary drawbacks are their long charging times and huge battery loads [2]. A portable recharge system was characterized as the photovoltaic recharge technique, while other solutions focused on developing supercharging stations that can fully recharge a car in under 30 minutes. The main issue is still the recharge time and capacity, especially for the solar system. Each method has its benefits and drawbacks. Drivers have positive reactions to the super-fast recharge stations in terms of the recharge time; nevertheless, this is not always advised, particularly in terms of battery security and durability[6]. Additionally, there is a risk of electrocution while using plugs, particularly in moist environments, and the lengthy line may raise safety concerns. Nowadays, wireless power charging is seen as the ideal answer to these issues. Numerous methods of transferring wireless energy were described in the literature, Capacitive power transfer, magnetic inductive power transfer, and magnetic resonant power transfer are the three main wireless power transmission technologies for battery charging. Dynamic wireless WPT offers the possibility of charging while moving. The transfer power efficiency of wireless charging systems, particularly during extended separation and misalignment, presents their greatest difficulty as compared to traditional methods [1][2]. Other methods described the idea of a recharger road, where a few wireless devices are installed into the road to transmit electricity. Vehicles will collect this energy and utilize it to recharge. This is how the wireless recharge system, which emerged after the year 2000, is conceptualized [6]. Because it can transmit more power at a faster pace than the CPT technique, the IPT method is preferred for charging EVs. Coupled magnetic resonance is thought to be an exception to the IPT. Approach, but one that transfers power over a medium distance. The DWPT system presented in this study uses the coupled magnetic resonance approach to transmit data at high frequencies up to 10MHz. DWPT systems based on coupled magnetic resonance offer a high-quality factor Q.85 kHz at 100 W to a resistive load[7]. A frequency is sent to another coil inside the automobile using high-frequency inverters with a coil attached underground. A converter is then used to flip this frequency from AC to DC. Electric wireless charging pathways are a creative way to charge quickly. The length of time it takes for automobiles to charge at today's electric stations is the biggest issue, which has an impact on the number of charging stations available. DWPT technology offers using grid-connected

charging stations that will wirelessly charge any moving object to address this issue. The vehicles will be equipped with in-built frequency receivers that enable them to pick up the frequency that the route transmits.

The Novelty of Approach

The concept that EVs with dynamic wireless charging systems may have significantly smaller batteries is probably the best benefit. As a result, this solution lowers costs and has a smaller negative impact on the environment, speeding up the adoption of electric vehicles. Urban Mobility is Simple.

II. WIRELESS POWER TRANSFER

In [2], the author designed a high-efficiency wi-fi energy switch system based on the magnetic resonant coupling to function at low frequency for electric automobile charging. It leads to an Impact on coil parameters (like coil span, curvature, and turns) and framework execution is evaluated using the 3D-finite element method. The author figure out that the device effectiveness and resonance frequency are impacted by the values of the coupling coefficient. The primary parameters are the quality factor (Q factor) of the coil, the coupling coefficient between coils, and the operating frequency. ANSYS Maxwell 3D is used for coils design and parameter estimation. He experimented that the power transfer efficiency changes with changing a coil span and the number of turns of the coil. The results show that a 3KW power transfer system with a 20cm distance and a 95% transfer efficiency was created. The system is designed to transfer 50KW with a 95% efficiency over 15cm of space. Also observed is that high-quality factors and increased performance are generated by a coil with a small inner diameter and a large number of turns for the same outer dimension. All parameters indirectly depend on the inner radius and no. of turns in a coil shown in (**table 1**) [2].

Table 1: Estimated parameters for different inner radii and number of turns

Inner radius(cm)	Number of turns	Self-inductance	Mutual inductance	Coupling coefficient	Q-factor	Efficiency
5	30	370.8	26.75	0.072	High	High
10	20	268.5	20.325	0.076	Medium	Medium
15	10	108.46	8.1	0.0757	Low	Low

In [3], the author's approach to a 3.7KW type-I wireless charger circular coil design modification was performed by applying 3D-finite element method analysis. The impact of various core characteristics on the coupling efficiency, the weight of the pads, and the mixture of fuel shielding by using the available ferrite cores as a model.

The wireframe model of the primary and secondary coil is shown in (**Figure 2**) [3].

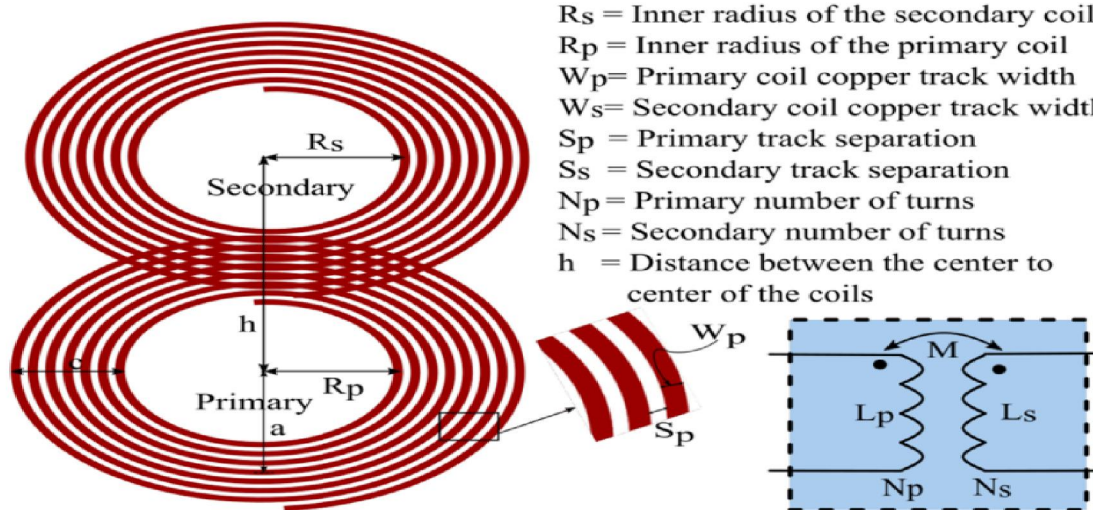


Figure 2: Primary and secondary coil interface of wireless power transfer

The impact of various core parameters on the coupling coefficient and weight of the pads, as well as flux shielding, has been examined using readily available ferrite cores as a reference. For 3.7KW output power, a circular pad measuring

450 mm x 450 mm is constructed. IPT(Inductive Power Transfer) systems can be made to be more productive, lightweight, and inexpensive by improving the pad design. Ansys Maxwell's 3-D FEM tool is used for the coil's whole design. Showing the flux density distribution in the core in (**Figure 3**) [3].

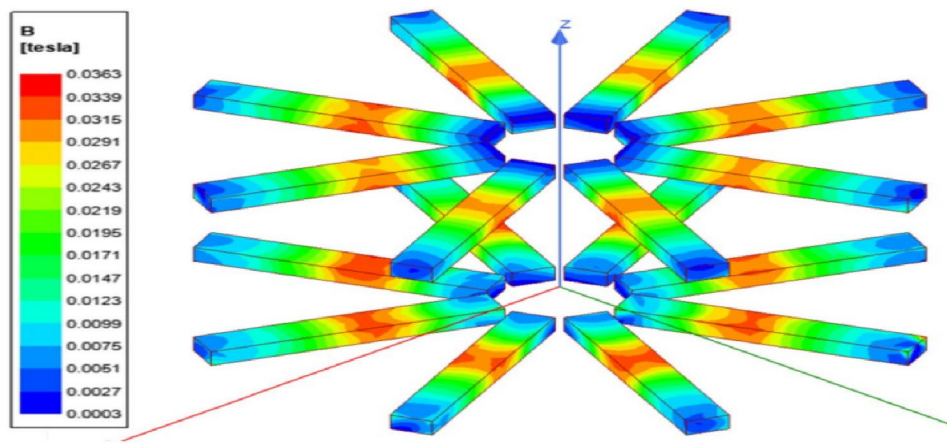


Figure 3: 3-D FEM simulation of the core showing the flux density distribution in the core of dimensions 186 mm \times 27 mm \times 16 mm

In [4], the authors are analyzed solve the control of a voltage stability wireless power transfer (WPT) charger for a battery-powered electric vehicle that is running in constant power charging mode. This shows the graph between the behavior of the backstepping controller versus the PI controller in (**Figure 4**) [4].

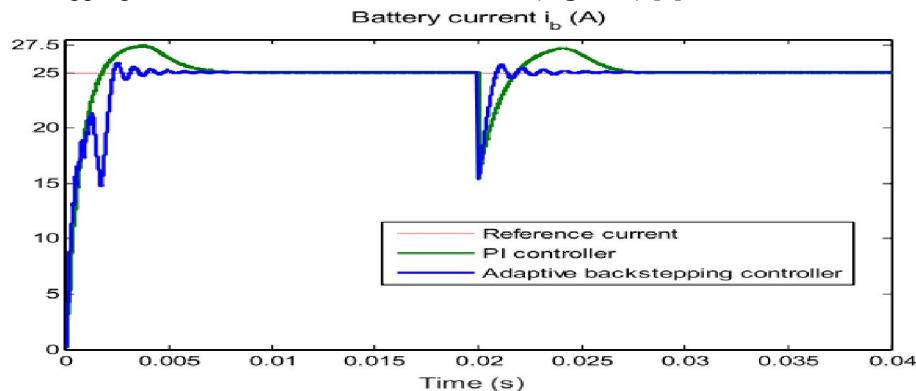


Figure 4: Behavior of the backstepping controller versus the PI controller during the transient regime

Authors identified that there are three challenges: Three factors- (1) The WPT charger model's extremely irregular terms, (2) Various condition parameters that cannot be measured, and (3) The identical model-all contribute to this conclusion is complex; additionally, its variables are undefined and subject to modify because of several causes including the battery age, operating temperature, and state of charge (SOC). They are followed to deal with all of these challenges with a combination of observer-based Kalman-like and coulomb counting estimation methods and a backstepping control approach to creating a nonlinear adaptive output feedback controller. Some goals are controlled they are tight management of the battery charging current, equilibrium stability of the closed circuit, and estimation of the WPT charger's system parameters. This section serves as an example and performance evaluation of the suggested nonlinear adaptive output feedback controller for the WPT charger. The results show that, numerous simulation models prove the effectiveness of the proposed control approach and that all control goals have been reached. And also observed that they noticed that the proposed approach shows good performance when compared it to a control approach based on a PI controller. That is, the MATLAB/Simulink program is used to model the global control system depicted in (**Figure 5**) [4].

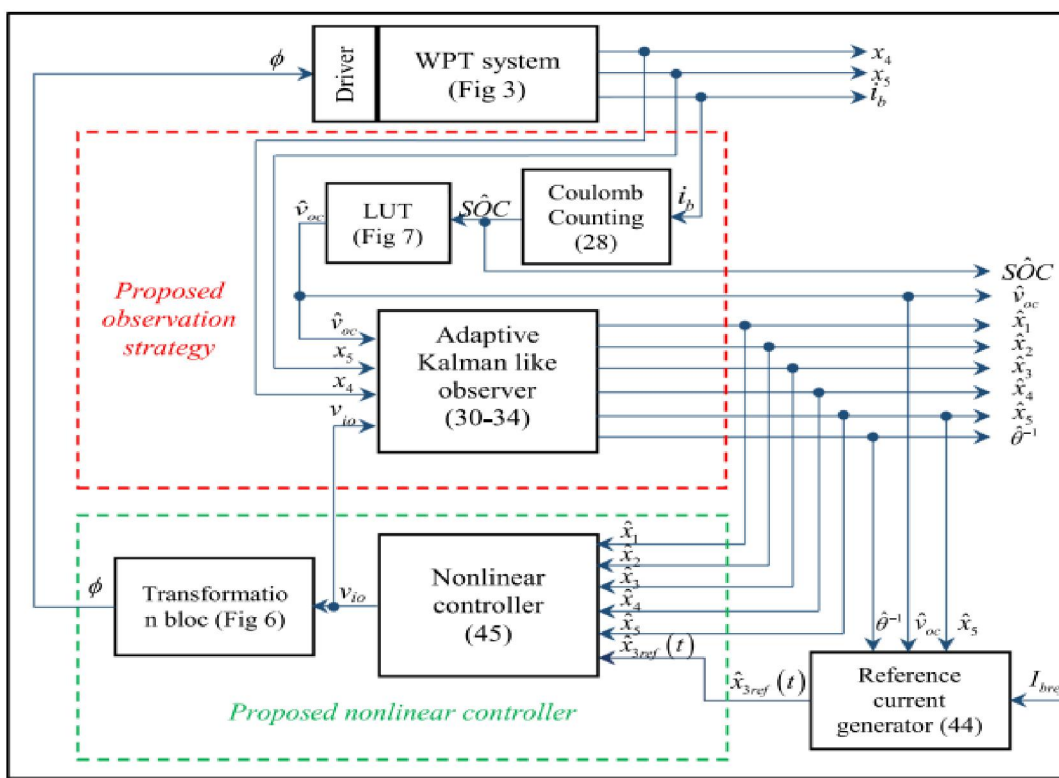


Figure 5: General structure of the proposed control strategy for the WPT charger

In [5], the Authors presented the design of a high-frequency transformer for use in electric car charging. This design experiments with numerous transformer designs with variable separations between the primary and secondary coils for wireless power transfer factors such as coupling efficiency and mutual inductance. They simulated the design by using ANSYS Maxwell software. The initial distance of separation is taken as 50mm and is gradually increased to 100mm. This test has been performed to verify the relation between the coupling coefficient and separation distance during electric vehicles' charging.

Table 2: Simulation results of circular coreless transformer with uniform coils

Arrangement type	The distance of separation (mm)	Coupling coefficient K	Inductance		
			L _{p(μH)}	M(μH)	L _{s(μH)}
Circular with uniform coils	50	0.470265	504.986518	231.990414	481.919660
	60	0.407312	506.768355	201.291490	481.932338
	70	0.353259	508.092388	174.805791	481.930341
	80	0.306738	508.884496	151.900615	481.907752
	90	0.2665780	509.363871	132.068972	481.893879
	100	0.231812	509.568603	114.873435	481.906772

The results show that when a larger coil has been used as the primary, a sufficient amount of supply voltage has been transferred to the secondary due to the large primary and small secondary coil. At a certain primary voltage, the quantity of energy delivered decreases with increasing distance. Simultaneously, if the distance between the coils is kept constant, the secondary coil's energy increases with the primary voltage. That the coupling between two coils increases as the distance of separation reduces.

Table 3: Simulation results of circular transformer model with non-uniform coils

Arrangement type	The distance of separation (mm)	Coupling coefficient K	Inductance		
			$L_p(\mu\text{H})$	M(μH)	$L_s(\mu\text{H})$
Circular with uniform coils	50	0.342476	136.622814	87.8786	481.927847
	60	0.295733	136.861185	75.949975	481.919172
	70	0.255525	137.067561	65.674876	481.943493
	80	0.220964	137.127711	56.802614	481.913621
	90	0.191176	137.179543	49.154552	481.914601
	100	0.165468	137.229701	42.553256	481.938353

III. COMPENSATION TOPOLOGIES

Since MIT proposed the concept of Magnetic Coupled Resonant Wireless Power Transmission (MCR - WPT) in 2007, the technology has advanced quickly and is now widely used in implantable medical devices, home appliances, mobile devices, and electric cars. Increased output power level is especially crucial for the Wireless Charging of Electric Vehicles. However, after the coil parameters are determined, the load resistance to achieve optimal efficiency of the SS topology WPT system is unchangeable, whereas the LCC topology can be modified according to the compensatory topology parameters.

Calculations are used to investigate and analyze the many electrical values present in an electrical circuit, particularly the nodal voltages and currents. In the Wireless Power Transfer (WPT) system, four resonant circuit topologies are used.

Series-Series (SS)

Series-Parallel (SP)

Parallel-Series (PS)

Parallel-Parallel (PP)

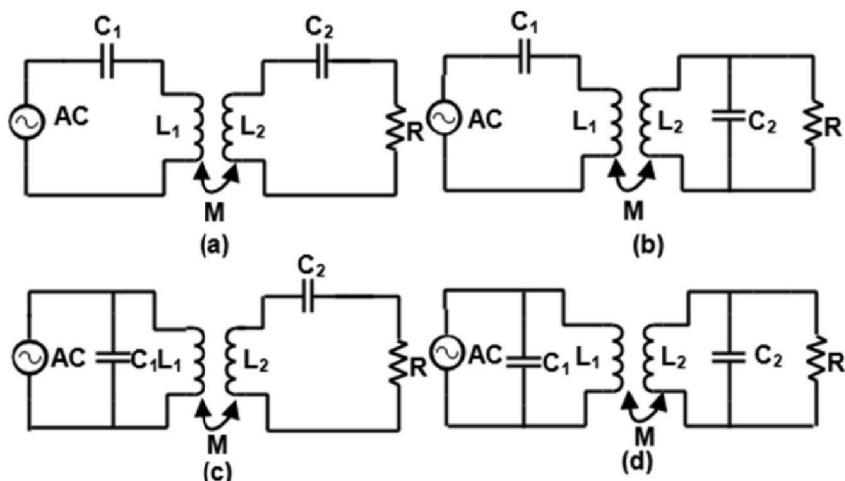


Figure 6: WPT topologies.

In addition to the four basic topologies described above, the hybrid-series-parallel (LCC, consisting of an inductor and two capacitors) compensation topology has received much attention due to its superior performance. It can perform Zero Phase Angle (ZPA) and Zero Voltage Switching (ZVS), and its output current is load-independent.

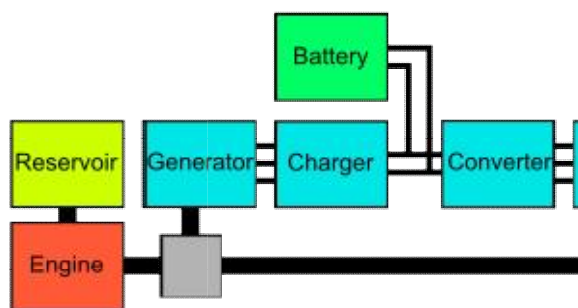


Figure 7: Model block diagram of a Wireless power transfer in an Electric car.

Table 4: WPT Topologies Specifications

Features	SS	SP	PS	PP
The sensitivity of the power factor over a distance	Low	Low	Moderate	Moderate
The impedance at the resonant state	Low	Low	High	High
Suitability for EV application	High	High	Moderate	Moderate
Power transfer capability	High	High	Low	Low
Alignment tolerance	High	High	Moderate	High
Frequency tolerance on efficiency	Low	High	Low	Low

Figure 7 depicts a schematic diagram of a magnetic coupled Wireless Power Transfer system in which AC power from the grid is rectified to form DC power, a high-frequency inverter is made up of an H-bridge, and transmits power to the receiver coil. The compensation topology used in primary and secondary compensation circuits is SS or LCC. Section 3 designed the transmitter and receiver coils, and the receiver end is connected to the electricity.

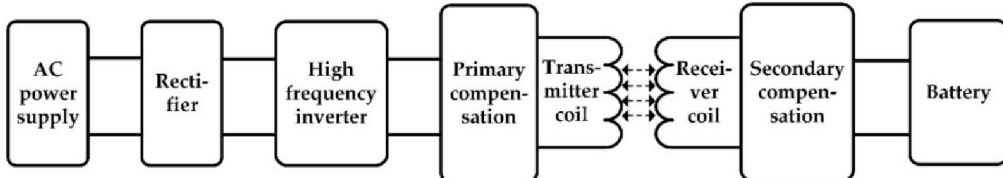


Figure 8: The structure diagram of the Wireless Power Transfer System.

Because the resonant part of the Wireless Power Transmission system includes bandpass filtering characteristics, only the fundamental wave component is examined afterward. The square wave created by the full-bridge inverter can be theoretically equal to an AC voltage source. The Fourier series is used to extend the square wave, the duty cycle is set to D, and the fundamental wave of the square wave has an amplitude of U_d :

$$F_t = (4U_d/\pi) \sin(\pi D) \cos(\omega t - \pi D) \quad \dots \quad (1)$$

To determine the number of turns, the coil parameters are properly constructed to provide a high-efficiency transmission system that meets the power requirements.

The most fundamental resonance structure is the SS topology. Series resonance is used on both the primary and secondary sides. Figure 4 depicts the equivalent circuit, where U_s is a voltage-stabilized source, the source internal resistance is ignored, and M is the mutual inductance between two coils.

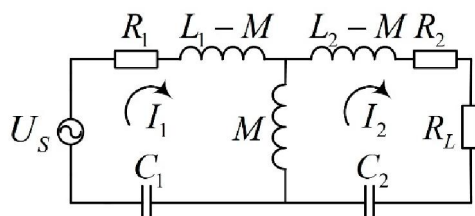


Figure 9: The equivalent circuit model of SS-type

According to Figure 4 and Kirchhoff Voltage Law (KVL), we can obtain:

$$\left\{ \begin{array}{l} (R_1 + j\omega L_1 + \frac{1}{j\omega C_1})I_1 - j\omega M I_2 = U_s \\ (R_2 + R_L + j\omega L_2 + \frac{1}{j\omega C_2})I_2 - j\omega M I_1 = 0 \end{array} \right. \quad \text{---(2)}$$

$$\left\{ \begin{array}{l} (R_1 + j\omega L_1 + \frac{1}{j\omega C_1})I_1 - j\omega M I_2 = U_s \\ (R_2 + R_L + j\omega L_2 + \frac{1}{j\omega C_2})I_2 - j\omega M I_1 = 0 \end{array} \right. \quad \text{---(3)}$$

When the system meets the resonance conditions:

$$f_0 = \frac{1}{2\pi\sqrt{L_1C_1}} = \frac{1}{2\pi\sqrt{\frac{1}{\omega M}}} \quad \text{---(4)}$$

When R_L is much greater than R_1 and R_2 , R_1 and R_2 can be ignored, the currents are as follows:

$$\left\{ \begin{array}{l} I_1 = \frac{U_s R_L}{(\omega M)^2} \\ I_2 = \frac{U_s}{\omega M} \end{array} \right. \quad \text{---(5)}$$

The transmission power and efficiency of the system are:

$$P_{ss} = \frac{U_s^2 R_L}{(\omega M)^2} \quad \text{---(6)}$$

$$\eta_{ss} = 1 - \frac{R_L R_1}{(\omega M)^2} - \frac{R_2}{R_L} \quad \text{---(7)}$$

The maximum transmission power and efficiency of the system are:

$$\eta_{ss_max} = 1 - \frac{2\sqrt{R_1 R_2}}{\omega M} \quad \text{---(8)}$$

$$R_{ss} = \sqrt{\frac{R_2}{R_1} (\omega M)^2} \quad \text{---(9)}$$

Because of this inverse relationship between distance and mutual inductance, it is usual in practical applications for the charging object to be located far away from the primary coil. According to (6) and (7), when the secondary side is open, the primary current increases significantly, when the secondary side is shorted, the primary current and transmission power fall. In the case of the SS structure with constant coil specifications, on the other hand, the load resistance to achieve optimal efficiency remains unchanging.

A new type of composite resonant structure is the LCC structure. L_{f1} , C_1 , C_{p1} and L_{f2} , C_2 , C_{p2} are the matching resonant circuit units of primary and secondary coils, as shown in Figure 5.

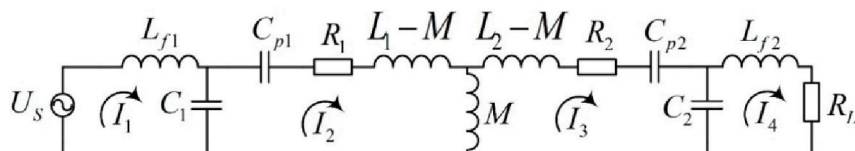


Figure 10: The equivalent circuit model of LCC - type.

Similarly, we can formulate the KVL equation according to Figure 5:

$$\begin{cases} (j\omega L_{f1} + \frac{1}{j\omega C_1})I_1 - \frac{1}{j\omega C_1}I_2 = U_s \\ (R_1 + j\omega L_1 + \frac{1}{j\omega C_1} + \frac{1}{j\omega C_{p1}})I_2 - \frac{1}{j\omega C_1}I_1 - j\omega M I_3 = 0 \\ (R_2 + j\omega L_2 + \frac{1}{j\omega C_2} + \frac{1}{j\omega C_{p2}})I_3 - \frac{1}{j\omega C_2}I_4 - j\omega M I_2 = 0 \\ (R_L + j\omega L_{f2} + \frac{1}{j\omega C_2})I_4 - \frac{1}{j\omega C_2}I_3 = 0 \end{cases} \quad \text{---(10)}$$

The resonance conditions are as follows:

$$\begin{aligned} C_1 &= \frac{1}{\omega^2 L_{f1}}, C_{p1} = \frac{1}{\omega^2 L_1 - \frac{1}{C_1}}, \\ C_2 &= \frac{1}{\omega^2 L_{f2}}, C_{p2} = \frac{1}{\omega^2 L_2 - \frac{1}{C_2}} \end{aligned} \quad \text{---(11)}$$

The currents of the loops are:

$$\begin{cases} I_1 = \omega^6 C_1^2 C_2^2 M^2 R_L U_s \\ I_2 = -\omega C_1 U_s \\ I_3 = \omega^4 C_1 C_2^2 M R_L U_s \\ I_4 = -\omega^3 C_1 C_2 M U_s \end{cases} \quad \text{---(12)}$$

The transmission power and efficiency of the system are:

$$P_{LCC} = \frac{M^2 U_s^2 R_L}{\omega^2 L_{f1}^2 L_{f2}^2} \quad \text{---(13)}$$

$$\eta_{LCC} = 1 - \frac{R_1 L_{f2}^2}{R_L M^2} - \frac{R_2 R_L}{\omega^2 L_{f2}^2} \quad \text{---(14)}$$

The maximum efficiency and corresponding load values are:

$$\eta_{LCC_max} = 1 - \frac{2 \sqrt{R_1 R_2}}{\omega M} \quad \text{---(15)}$$

$$R_{LCC} = \sqrt{\frac{R_1 \omega^2 L_{f2}^4}{R_2 M^2}} = \frac{R_1 L_{f2}^2}{R_2 M^2} R_{SS} \quad \text{---(16)}$$

The inductive coupler of an IPT system for supplying 6.6kW, 500V to an EV battery pack through 25cm of an air gap was designated as two identical square coils in the transmitter and receiver sides, with a ferrite plate behind each coil. The parameters of the inductive coupler were found using Finite Element Analysis (FEA) in ANSYS Maxwell. MATLAB technical computing software was used to calculate the resonant circuit parameters and inverter input DC voltage (Vin), and the equivalent circuit was then implemented in the PSIM simulation software. An EV battery pack was modeled as a resistive load in the work (RL). This representation is solely applicable in a steady-state analysis.

$$R_e = \begin{cases} \frac{8}{\pi^2} R_L & \text{for series secondary compensation} \\ \frac{\pi^2}{8} R_L & \text{for parallel secondary compensation} \end{cases} \quad \text{---(17)}$$

The above equation gives the comparable Effective Resistance (Re) (that indicates the loading effect of the EV batteries) on the power source. FEAANSYS Maxwell was used to find the parameters that define the inductive coupler and misalignment (L1, L2, and M). This part gave the PSIM simulation results of the analysis and comparison criteria between the four resonant topologies. The square coils design parameters and system specification are listed in Table 2 below;

Table 5: The coils design parameters and system specification.

Parameter	N ₁	N ₂	L ₁ (μ H)	L ₂ (μ H)	M(μ H)	d (cm)
Value	30	30	524.44	526.25	129.14	25

Table 6 shows the measured highlight values for L₁ and L₂ as well as M. The measured values of L₁ and L₂ were inconsistent; this little inaccuracy must be caused by computer constraints.

Table 6: The highlight values of L₁, L₂, and M due to the misalignment conditions.

Parameter <i>Highlight condition</i>	$\Delta L=30\text{cm}$	$d=30\text{cm}$	$\alpha=10^\circ$	well aligned case	$\theta=60^\circ$	$d=20\text{cm}$
L ₁ (μ H)	529.35	521.16	527.03	524.44	527.71	540.5
L ₂ (μ H)	538.31	531.5	533.77	526.25	535.35	546
M (μ H)	35	95.4	123.23	129.14	131	185.7

The inductively coupled coils were simulated in the FEA ANSYS Maxwell at air gaps d = 10, 15, 20, 25, 30, and 50 cm. The measured parameters (L₁, L₂, and M) for each d were inserted into MATLAB to compute the corresponding resonance parameters of each resonance circuit at 20kHz. Then all parameters were inserted into PSIM, and the input impedance ($Z_{in}=V_{in}/I_{in}$) and the dc-dc efficiency ($\eta=P_{out}/P_{in}$) of the SS, SP, SPS, and dual side LCC circuit topologies were determined.

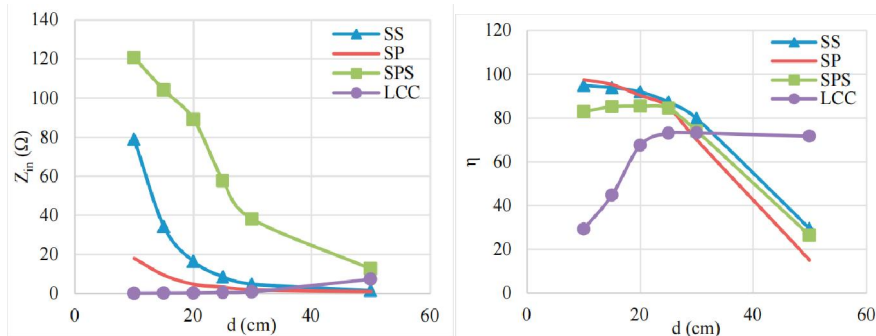


Figure 11: Effect of d on the (a) Z_{in} ; (b) η .

The results show that the SS topology is the most efficient in small air-gap applications, whereas dual-side LCC is useful in big air-gap applications. Based on the high VL required to power a battery during fast charging, the SP is the most efficient topology among the others.

Table 7: Characteristics and comparison of various compensation topologies.

Parameters	Topology				
	Z _{in}	high	low	very high	very low
suitability for small/large d	small (d<30cm)	small (d<30cm)	small (d<30cm)	large (d>30cm)	
ability to supply low/high V _L	η slightly decreases as V _L increases	η significantly increases as V _L increases	supply max V _L at resonance condition	η decreases as V _L increases	
G _V	low	slightly high	very low	very high	
sensitivity to misalignment	d (25cm±5) $\Delta L (\pm 30\text{cm})$ $\theta (\pm 60^\circ)$ $\alpha (\pm 15)$	sensitive slightly sensitive insensitive insensitive	sensitive very sensitive insensitive sensitive	sensitive very sensitive insensitive insensitive	very sensitive very sensitive very sensitive very sensitive
activity at low/high f	proportional to 1/f	proportional to 1/f	proportional to 1/f	proportional to 1/f	proportional to 1/f

Figure 11 shows the classification of the compensation topology. They include two groups. The first is of the four basic topologies and the second comprises hybrid topologies, which are combinations of series and parallel topologies.

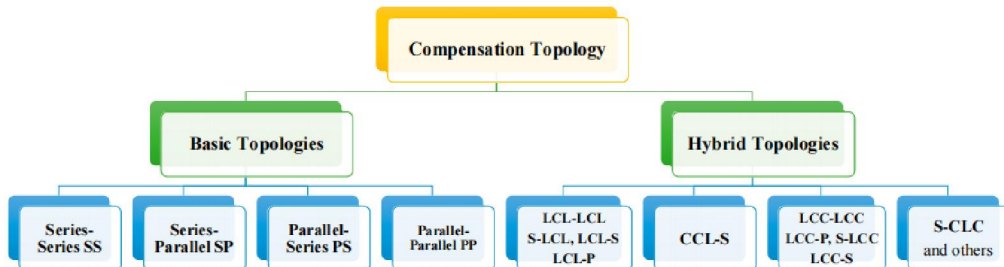


Figure 12: Classifications of the compensation topology

Some commonly used hybrid topologies in the research work are displayed in Figure 12. L_p and L_s are the primary and secondary inductances, respectively.

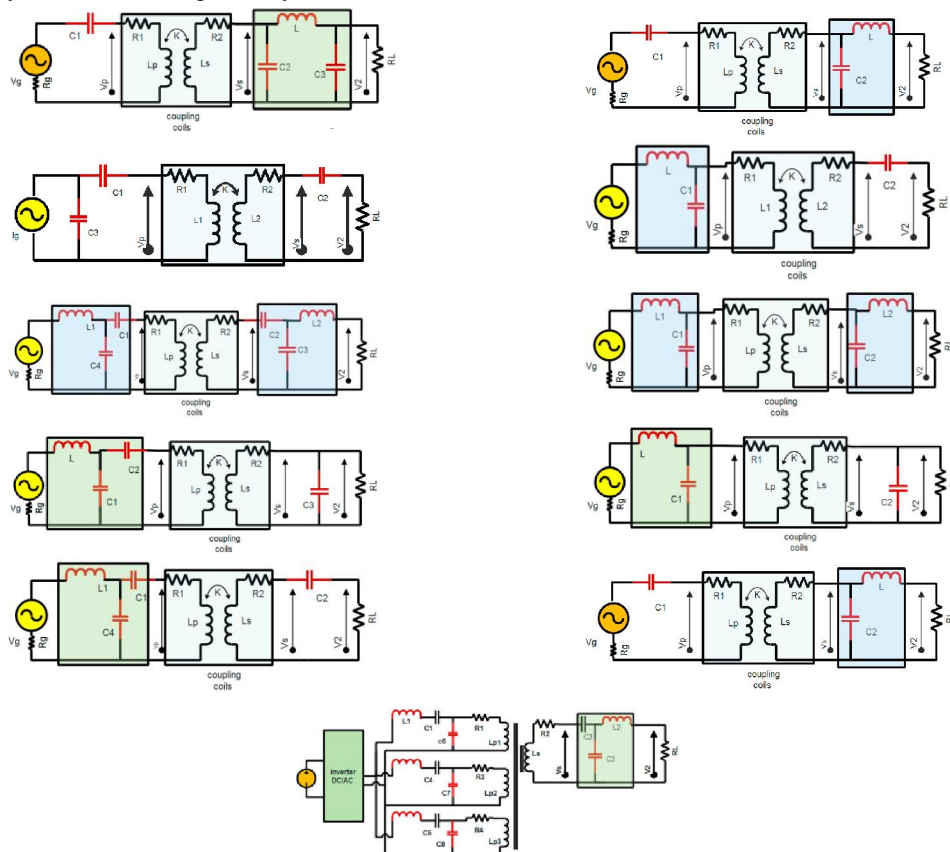


Figure 13: Hybrid compensation topologies:

- (a) S-CLC, (b) S-LCL, (c) CCL-S, (d) LCL-S, (e) LCC-LCC, (f) LCL-LCL, (g) LCC-P, (h) LCL-P, (i) LCC-S, (j) S-LCL, (k) Double-Sided LCC

Table 8: Review of different WPT systems based on topology and application type (such as electric vehicles, or EVs).
EMI: Electromagnetic Field Interference.

Reference and Topology	f_0/kR_L (kHz, Ω)	P_{out}, V_{out}	Efficiency	N_1 Turn N_2 Turn	Resonators D ₁ mm Length, Diameter mm	D ₂ mm width, Diameter mm	Gap mm	Note
[14] SS/LCC-LCC	$f_0 = 85$ $k = 0.135$ $R_L = 2, 3, 5$	1 kW 50 V	95% for SS, and 93% for LCC	10 8	500 diameter	400 diameter	200	Based on EMI, LCC-LCC topology is considered more robust to EMI exposure.
[89] SS/LCC-LCC	$f_0 = 79$	7.7 kW max. 270–405 V	For LCC: 96%	-	800	600	200	The LCC-LCC topology has higher efficiency when the mutual inductance is at minimum.
[101] SS/LCL-LCL	$f_0 = 85$ $k = 0.1$ $R_L = 10$	3.3 kW	93.1% for SS, 89.5% for LCC	20 × 3 layers 17 × 2 layers	550 × 400 mm ²	240 × 240 mm ²	100	Compared to SS topology, the LCL-LCL type has a high power factor.
[98] LCC-LCC	$f_0 = 79$ $k = 0.18–0.32$ $R_L = 10–200$	7.5 kW 450 V	96%	1	800	600	200	Resonant frequency f_0 is independent of the coupling coefficient and load conditions.
[99] LCC-LCC	$f_0 = 95$ $k = 0.14–0.30$	5.6 kW 300–450 V	95.36%	-	600 200	600 200	150	The extra integration-induced couplings give more space for magnetic cores.
[87] LCC-LCC	$f_0 = 85$ $k = 0.153$ $R_L = 49.95$	3.3 kW 405.7 V	92.6%	18 16	600	300	150	Energy storage has no relation to topology type, but only with transferred power level and coupling coefficient.
[97] LCC-LCC	$f_0 = 85$ $k = 0.1877$	3 kW 300 V	95.5%	-	600 × 450 × 4 mm ³ 640 × 496 × 8 mm ³ 711.2 × 558.8 × 2 mm ³	400 × 300 × 4 mm ³ 480 × 352 × 8 mm ³ 508 × 406 × 2 mm ³	150	The compensated resonator design helps to eliminate or reduce the extra-coupling effects to a tiny level.

Table 9: Review of WPT systems that are used in dynamic charging for EVs and plug-in hybrid electric vehicles (PHEVs).

Reference and Topology	f_0/kR_L (kHz, Ω)	P_{out}, V_{out}	Efficiency	Coils' Dimensions and Number of Turns	Gap mm	Note
[96] LCL-S LCC-S	$f_0 = 140$ $k = 0.18–0.32$	Nominal power: 1 kW 80–90 V	Similar: LCC and LCL: 93%	Coil radius is 163 mm	100	The topology gives more robust power transfer character against the variation of k .
[100] Double-sided LCC	$f_0 = 85$ $k = 0.13$	1.4 kW 150 V	89.78%	9 turns for each transmitter, Tx coil 6 × (388 mm × 400 mm), and for Rx: 485 mm × 400 mm	150	This paper presented a continuous dynamic WPT system, which reduces the power pulsations.
[102] LCL	$f_0 = 85$ $k = 3.7–5.4\%$	5 kW	-	The secondary: 0.35 m × 0.7 m N87 ferrite material (each 93 mm × 28 mm × 16 mm).	240	The system is designed to supply power along the whole length of the track by activating only one primary pad.
[103] SS	$f_0 = 85$ $k = 0.4$	20 kW	80%	Transmitter dimensions are 10 cm × 75 cm, number of turns: nine Receiver: 25 cm × 20 cm, number of turns: 12.	100	Downscale prototype operating at 85 kHz ± 2.5 kHz.
[104] SP	$f_0 = 23$ $R_L = 2$	2 kW	-	Coils diameter: 330 mm. Turns: seven turns for transmitter coil and five turns for receiver coil.	100	This paper presented technical aspects of in-motion WPTs for charging EVs and PHEVs.
[105] SS	$f_0 = 85$	-	97.6% pads length ratio is 1:1	Coil external width: 58 mm Coil inner width 38 Wire diameter 5 mm Number of turns: 8 turns.	200	Investigated the pad shape: influence of the variation of the ratio between Tx and Rx lengths with respect to the behavior of the coupling.

The Application of class-c amplifier to WPT circuit is very limited, but there is three paper on class-c amplifier function in WPT circuit which only use P-P resonant tank with different parts, which can see in Table 6.

Table 10:

Article	Topologies	Efficiency (%)	Part of Efficiency
[3]	P-P	43	drain-efficiency
[4]	P-P	97.3	class-c amplifier
[5]	P-P	90	link efficiency

Many papers have already been published on WPT circuits using the near-field approach, with many of them using class-d and class-e power amplifiers as oscillator circuits due to their great efficiency. Furthermore, the WPT compensation circuits employ four distant topologies: (P-P), (P-S), (S-P), and (S-S). They presented a modification of class-c Wireless Power Transfer and compared the results for four resonant tank topologies to determine which is the best for a class-c amplifier. According to the power matters alliance (PMA) guidelines, the resonant frequency from the WPT circuit is 205300kHz. Furthermore, the WPT circuit is based on the rules of the Broadband Wireless Forum (BWF) Japan, which include 10 kHz to 10 MHz, the transmitter power is less than 50 W, and the power transmitter distance not exceeding several meters.

IV. PROPOSED CIRCUIT

4.1 Transmitter Circuit

This section is divided into three sections: the class-s amplifier as the oscillator circuit, the LTC69992 as the input for the gate drive MOSFET, and the resonant tank. Figure 9 shows the transmitter circuit. A class-C topology is an appealing option for low-power applications. In a typical operation, a high-amplitude input signal is applied to the gate of the n-MOSFET, causing it to conduct a drain current (i_d). LTC69992 can generate a square wave signal with a 50% duty cycle for gate drive n-MOSFET signals. It can be controlled using Pulse Width Modulation (PWM) in the modulation port ranging from 0 V to 1 V. Furthermore, the LTC69992 has a resonant LCT69992 frequency range of 3.81 Hz to 1 MHz. LTC69992 frequency can be calculated using (18).

$$f_{out} = \frac{1MHz \times 50k\Omega}{N_{div} \times R_{set}} \quad \text{----- (18)}$$

f_{out} is the frequency output, N_{div} is the number of div codes based on the data sheet that split in the resonant frequency target, and R_{set} is the value of the resistor used to set the voltage from the modulation port, which is modified by half of the R_{set} . The highest frequency result from LTC69992 is 1 MHz. Figure 1 depicts the gate drive design for a resonance frequency of 250 kHz.

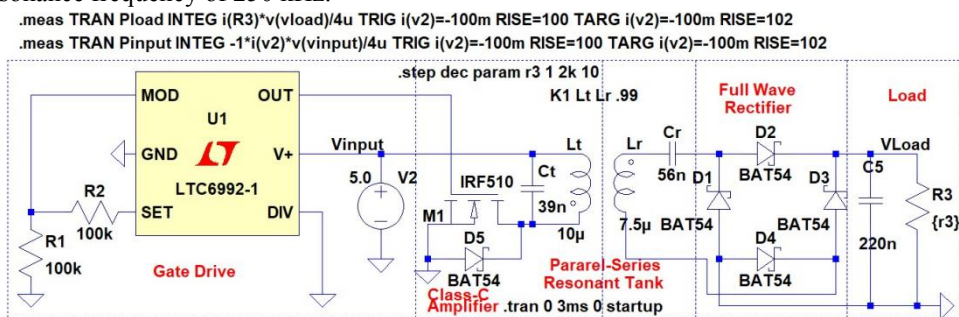


Figure 14: Class-C WPT circuit with P-S topologies.

4.2 Resonant Circuit

The values of the inductor and capacitor resonant tank in the transmitter and receiver can resolve by (19) and (20)

$$f_t = \frac{1}{2\pi\sqrt{L_t C_t}} \quad \text{----- (19)}$$

$$f_r = \frac{1}{2\pi\sqrt{L_r C_r}} \quad \text{----- (20)}$$

where f_t is the resonant frequency in the transmitter,

L_t is the value inductor transmitter,

C_t is the value capacitor transmitter,

f_r is the resonant frequency in the receiver,

L_r is the value inductor transmitter,

C_r is the value capacitor receiver.

Based on the calculation the resonant frequency is 250 kHz.

4.3 Receiver Circuit

This part can divide into 3 sections, resonant tank, rectifier, and load. The rectifier uses a full wave rectifier with bat 54 Schottky diode because this module has a forward current of 0.3 A. The load use resistor the value can be changed.

V. SIMULATION RESULT AND DISCUSSION

The transmitter and receiver parts are separated by an air gap. The simulation employed the LT spice transient analysis directive till 3 ms(.tran 0 3 ms 0 start up) and the coupling coefficient (k) directive ($K1 Lt Lr.99$) between the transmitter and receiver inductors (L_r). K ranges from 0 to 0.99, with a 0.1 increment. The simulation additionally

makes use of the step parameter command to adjust the value of the load resistor from 1 to 2k depending on the sweep decade. The voltage input (V input) and voltage output in the (V load) are obtained from loads 1- 2 k and 0.99, respectively. When 2 ms passes the WPT circuit begins to work. Figure 10 depicts the power efficiency of P-P, S-S, S-P, and P-P. The power efficiency (η) is calculated as (21). With values of 0.54 watts and 0.17 watts, respectively, the P-S topologies have the maximum input and power. S-P and S-S topologies, on the other hand, have the lowest efficiency because their output voltage is only about 0 at K 0.99. Because V load and current load have multiple ripple outputs based on simulation, power efficiency in load has multiple ripple outputs based on simulation, and power efficiency in load is measured using the power root mean square (r.m.s) formula.

The power efficiency is measured using the LT spice measure command, as shown in Figure 9, for example in load (.meas TRAN Pload INTEG I (R3)*v(V load)/4uTRIG I (v2)=-100m RISE=100 TARGI (v2)=-100m RISE=102). It employs integ (integral), rises 100, and rises 102 as amplitudes, and tran as a transient analysis technique.

$$\eta = \frac{P_{Load}}{P_{input}} = \frac{\frac{1}{T} \int_{T_1}^{T_2} V_{Load} \times I_{Load} dT}{\frac{1}{T} \int_{T_1}^{T_2} V_{input} \times I_{input} dT} \quad \text{-----(21)}$$

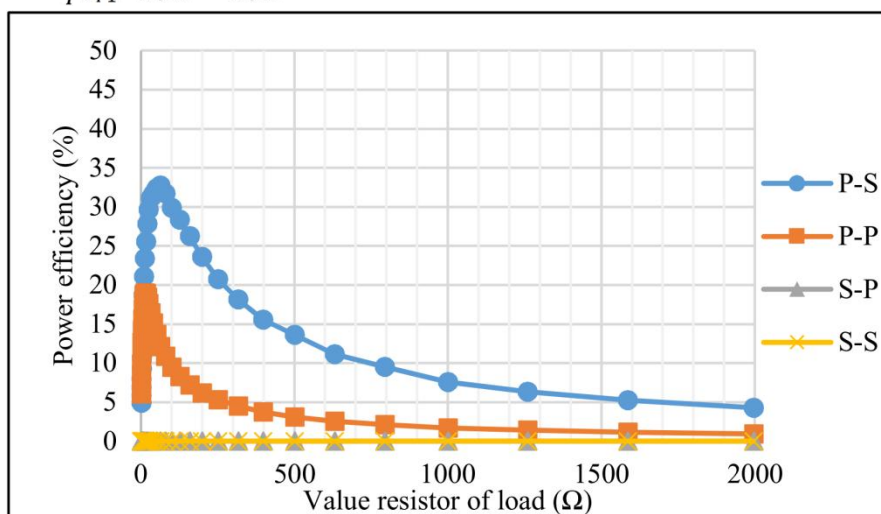


Figure 15: Power efficiency vs resistor of load proposed circuit.

VI. CONCLUSION

(Shehata, 2022) Higher quality factor and transfer efficiency are developed for coils with tiny inner diameters and many turns for the same outside dimension. Mutual coupling occurs over tiny distances between coils. Coil self-inductance varies in the space between coil turns. The separation between the transmitter and receiver also affects the resonance frequency. While the resonance frequency relies on coupling coefficient at low spacing, the self-inductance is constant at high spacing. The effectiveness of the double-sided LCC compensation topology is higher at high coupling coefficients than that of the S-S compensation topology. Higher voltage stress is present with S-S correction, though.

(Yakala et al., 2021) Results from simulations and measurements for the a power pad of 450 mm by 450 mm is compared. For various horizontal and vertical misalignments. The 3.7 kW of power can be transferred via the designed power pad. Up to its full strength at a 100 mm charging zone, 150 mm vertical of set stress.

(Lassioui et al., 2021) We discovered that the suggested strategy exhibits good performances when we compared it to a control approach based on a PI controller. Additionally, we discovered that the PI control approach is only based on the input/output information of the charger, while the internal information is typically lacking, when comparing the two control approaches according to their capacity to give a deep understanding of the evolution of the charger's internal signals.

(Kathirvelu et al., 2021) Design outcomes demonstrate that self-impact inductance's on WPT has been overcome by the significant air gap that is built-in to the system. Additionally, simulation studies reveal that the coupling between two coils rises as separation distance does reduces.

(Zhang et al., 2019) A 3D electromagnetic field simulation with all parameters set in accordance with the most recent design from ORNL was conducted to calculate the electromagnetic emission in high power WPT, with the one-point magnetic field being confirmed by measurement from ORNL. According to the results of the simulation, electromagnetic safety would become a serious problem if the power reaches 150 kW and above.

REFERENCES

- [1] N. Mohamed *et al.*, “A new wireless charging system for electric vehicles using two receiver coils,” *Ain Shams Eng. J.*, vol. 13, no. 2, p. 101569, 2022, doi: 10.1016/j.asej.2021.08.012.
- [2] E. G. Shehata, “Design of high efficiency low frequency wireless power transfer system for electric vehicle charging,” *Electr. Eng.*, vol. 104, no. 3, pp. 1797–1809, Jun. 2022, doi: 10.1007/s00202-021-01436-w.
- [3] R. K. Yakala, S. Pramanick, D. P. Nayak, and M. Kumar, “Optimization of Circular Coil Design for Wireless Power Transfer System in Electric Vehicle Battery Charging Applications,” *Trans. Indian Natl. Acad. Eng.*, vol. 6, no. 3, pp. 765–774, Sep. 2021, doi: 10.1007/s41403-021-00224-z.
- [4] A. Lassioui, H. EL Fadil, A. Rachid, T. Bouanou, and F. Giri, “Adaptive Output Feedback Nonlinear Control of a Wireless Power Transfer Charger for Battery Electric Vehicle,” *J. Control. Autom. Electr. Syst.*, vol. 32, no. 2, pp. 492–506, Apr. 2021, doi: 10.1007/s40313-020-00670-0.
- [5] K. P. Kathirvelu, G. G. V. Sandeep, J. Swathi, R. Amirtharajan, and R. Balasubramanian, “Design of Transformer for Wireless Power Transfer in Electric Vehicles,” *Iran. J. Sci. Technol. - Trans. Electr. Eng.*, vol. 45, no. 4, pp. 1311–1324, Dec. 2021, doi: 10.1007/s40998-021-00441-w.
- [6] N. Mohamed, F. Aymen, M. Ben Hamed, and S. Lassaad, “Analysis of battery-EV state of charge for a dynamic wireless charging system,” *Energy Storage*, vol. 2, no. 2, pp. 1–10, 2020, doi: 10.1002/est2.117.
- [7] A. Rakhymbay, A. Khamitov, M. Bagheri, B. Alimkhanuly, M. Lu, and T. Phung, “Precise analysis on mutual inductance variation in dynamic wireless charging of electric vehicle,” *Energies*, vol. 11, no. 3, 2018, doi: 10.3390/en11030624.
- [8] M. Al-Saadi, A. Ibrahim, A. Al-Omari, A. Al-Gizi, and A. Craciunescu, “Analysis and Comparison of Resonance Topologies in 6.6kW Inductive Wireless Charging for Electric Vehicles Batteries,” *Procedia Manuf.*, vol. 32, pp. 426–433, 2019, doi: 10.1016/j.promfg.2019.02.236.
- [9] M. A. Houran, X. Yang, and W. Chen, “Magnetically coupled resonance wpt: Review of compensation topologies, resonator structures with misalignment, and emi diagnostics,” *Electron.*, vol. 7, no. 11, 2018, doi: 10.3390/electronics7110296.
- [10] I. Sukma and A. Kitagawa, “Comparison Topologies of Resonant Tank from Class-C Wireless Power Transfer,” *2018 IEEE Int. Work. Electromagn. Appl. Student Innov. Compet. iWEM 2018*, no. August, 2018, doi: 10.1109/iWEM.2018.8536684.
- [11] F. Wen, X. Chu, Q. Li, and W. Gu, “Compensation parameters optimization of wireless power transfer for electric vehicles,” *Electron.*, vol. 9, no. 5, pp. 1–12, 2020, doi: 10.3390/electronics9050789.